JCTC Journal of Chemical Theory and Computation

Article

pubs.acs.org/JCTC

Excited-State Tautomerization of 7-Azaindole in Nonpolar Solution: A Theoretical Study Based on Liquid-Phase Potential Surfaces of Mean Force

Hua Fang and Yongho Kim*

Department of Applied Chemistry, Kyung Hee University, 1 Seochun-Dong, Giheung-Gu, Yongin-Si, Gyeonggi-Do, 446-701, Republic of Korea

Supporting Information

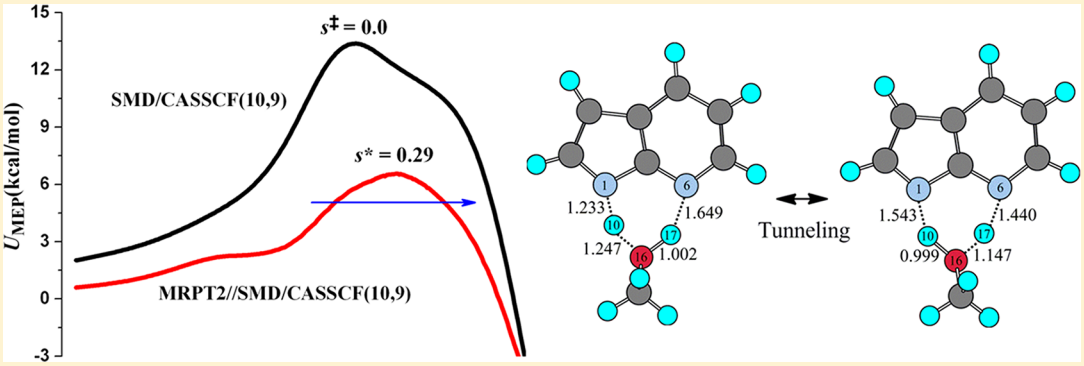

ABSTRACT: Excited state tautomerization of a 7-azaindole (7AI) complex with one methanol molecule in heptane was studied using variational transition state theory including multidimensional tunneling (VTST/MT) with the dielectric continuum model for the solvent effect. Electronic structures and energies for reactants and transition state (TS) in solution were computed at the complete active space self-consistent field (CASSCF) level with second-order multireference perturbation theory (MRPT2) to take into consideration of dynamic electron correlation. The polarizable continuum model using the integral equation formalism (IEFPCM) and the SMD model were used for the excited-state solvent effect. Excited-state surfaces of potential of the mean force in solution were generated for the first time at the MRPT2//SMD/CASSCF(10,9)/6-31G(d,p) level. The position of TS on the reaction coordinate substantially depended on the dynamic electron correlation. The two protons in the excited-state tautomerization were transferred in a concerted but asynchronous process. Calculated HH/DD kinetic isotope effect (KIE) and the ratio of Arrhenius pre-exponential factors, A(HH)/A(DD), agreed very well with the corresponding experimental values. The shape of the adiabatic energy surfaces in the excited-state strongly depended on the position of isotopes due to the asynchronicity of the reaction path, and the tunneling effect was essential for reproducing experimental KIEs. The pyrrolic proton moved a twice longer distance by tunneling than the hydroxyl proton in the most probable tunneling path at 292 K. This study strongly suggests that the mechanism of the excited-state double proton transfer in heptane is triggered by proton transfer from the pyrrolic nitrogen of 7AI to alcohol (protolytic pathway), rather than by proton transfer from alcohol to the pyridine nitrogen of 7AI (solvolytic pathway).

1. INTRODUCTION

Proton transfer is one of the most common and fundamental chemical reactions and plays an important role in a wide variety of biological and chemical phenomena.[1−8] In biological systems, proton transfer usually takes place over long distances through hydrogen-bonded networks that can act as an effective pathway for rapid migration of protons. In order to understand this phenomenon, it is essential to investigate the dynamics of solvent-mediated long-range proton transfer, which is determined by the size, structure, and motions of mediating solvent molecules.[7] Because it is extremely difficult to explore proton-relay dynamics directly in biological systems due to the structural complexity,[4−7] it is necessary to establish simplified models. One of the most frequently studied systems for proton transfer is 7-azaindole (7AI), which contains one proton donor (N−H) and one proton acceptor (=N−) that provide simple hydrogen-bonded structures upon complexation with polar solvents.

The excited state tautomerization of 7AI-alcohol complexes in the gas phase and in solution has been extensively studied to mimic proton transfer dynamics in complicated molecular systems such as enzymes and proteins. Recently, excited state multiple-proton transfer reactions in 7AI-(Solvent)$_n$ (n = 1 − 3; Solvent = H_2O/CH_3OH/C_2H_5OH) complexes[9−13] have been studied in the gas phase. A series of studies on 7AI-(H_2O/

Received: December 6, 2012
Published: July 3, 2013

$CH_3OH/C_2H_5OH)_n$ (n = 1 − 3) indicated that multiple proton/hydrogen transfers are solvent and cluster-size dependent; only 1:2 complexes exhibited excited-state tautomerization by triple-proton transfer,[9−12] whereas no clear evidence for excited-state tautomerization in a 1:1 cluster has been observed. Pino et al.[14] have performed a picosecond pump and probe experiment and *ab intio* calculations for 7AI-$(H_2O)_{2,3}$ and suggested that the fast decay in 7AI-$(H_2O)_3$ could be related with the interconversion between "cyclic-nonplanar isomer" and "bridged planar isomer", and Yu et al.[15] theoretically showed that the excited quadruple proton transfer is very slow due to a high barrier and the excited triple-proton transfer occurs from cyclic-nonplanar structure. Daengngern et al.[16] have recently performed dynamics simulations for excited-state proton transfer reactions in 7AI-$(CH_3OH)_n$ (n = 1 − 3) complexes and reported that there are no crossings between $S_{\pi\pi^*}$ and $S_{\pi\sigma^*}$ states and two CH_3OH molecules assist the excited state triple-proton transfer.

The excited-state double proton transfer (ESDPT) of a 7AI-CH_3OH complex was observed in the condensed phase, and the excited state tautomerization of 7AI-CH_3OH has been discussed as a two-step model.[17]

Scheme 1

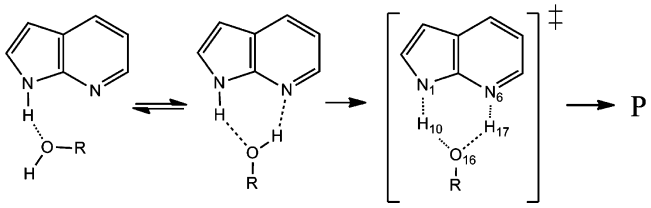

In this model, the first step involves solvent reorganization to form a cyclic H-bonded 7AI-CH_3OH complex, while the second step is an intrinsic double proton transfer. Intrinsic proton transfer is often presumed to be very fast and is governed by tunneling.[18,19] This model is widely accepted as the mechanism of ESDPT in 7AI-alcohol complexes in the condensed phase. If solvent motions were rate-limiting, no significant kinetic isotope effect (KIE) would be expected. However, KIEs for excited-state tautomerization have been observed in 7AI complexes with various alcohols.[20] Moog et al.[17] suggested that solvent reorganization and the intrinsic proton transfer step together determine the reaction rate. Chen et al.[21] reported that two protons were transferred in the excited-state tautomerization of 7AI in methanol based on proton inventory experiments and suggested a concerted mechanism for the intrinsic proton transfer step.

ESDPT reactions of the 7AI-CH_3OH complex in the gas phase and in methanol solution have recently been studied theoretically.[22,23] The excited state tautomerization process of the complex in both the gas phase and in solution were concerted but asynchronous, in which the proton translocated first from the pyrrole ring of 7AI to methanol, followed by rapid proton transfer from the $CH_3OH_2^+$ group to the pyridine N atom. However, Kwon et al.[20] reported that the ESDPT of 7AI-CH_3OH in nonpolar heptane was initially triggered by proton transfer from methanol to the pyridine nitrogen of 7AI, forming a cationic 7AI intermediate species, followed by rapid proton transfer from the pyrrole nitrogen of the intermediate to the transient alkoxide moiety. The ESDPT of the 7AI-CH_3OH complex in *n*-heptane occurs consecutively on a time scale of 88 ps with an unusually large, temperature-independent, and viscosity dependent KIE at 292 K. These authors also suggested that tunneling might depend on heavy-atom reorganization, which is required to reach the optimal pretunneling configuration. Heavy-atom vibration assisted tunneling is in principle identical to the large tunneling assisted by the breathing motion of an enzyme.[7,24−27] However, the role of heavy-atom reorganization in tunneling in relation with the detailed reaction dynamics have not yet been fully understood,[28−32] which is essential to explain such interesting experimental observations.

In the present paper, we report variational transition state theory calculations for the ESDPT in 7AI-CH_3OH in liquid phase. The structures and energies of the reactants, transition states (TS), and products were calculated and compared with experimental results in the gas phase and in heptane. The structures and energetics for the 7AI-C_2H_5OH complex were also calculated for comparison. The multidimensional excited-state surfaces of potential of mean force (PMF) for the 7AI-CH_3OH complex in heptane were generated for the first time using the interpolated variational transition state theory by mapping the (IVTST-M) method[33] at the complete active space self-consistent field (CASSCF) level with second-order multireference perturbation theory (MRPT2) to take into consideration of dynamic electron correlation and the SMD self-consistent reaction field model. The PMF and vibrationally adiabatic energy surfaces for isotopically substituted 7AI-CH_3OH complexes were also calculated. These adiabatic energy surfaces were used to calculate rate constants and KIEs using variational transition state theory including multidimensional tunneling (VTST/MT) approximations. The computed KIEs were compared with experimental results.

2. COMPUTATIONAL DETAILS

Reactant, product, and TS geometries of the excited state proton transfer reaction of 7AI-CH_3OH and 7AI-C_2H_5OH complexes in the gas phase and in heptane were fully optimized at the CASSCF level with the 6-31G(d,p) basis set using the Gaussian 09 program.[34] At the CASSCF level, the active space included four π bonds, four corresponding antibonding orbitals, and one nitrogen lone pair resulting in an active space of 10 electrons in 9 orbitals, which was denoted CASSCF(10,9). Vibrational frequencies were calculated at the same level. No imaginary frequencies for the reactant or product and one imaginary frequency for the TS verified the optimized structures. Single point energy calculations with the 6-31G(d,p) basis set were also performed using second-order multireference perturbation theory (MRPT2)[35−40] for stationary points. All MRPT2 calculations were performed using the GAMESS program.[41]

Continuum model calculations were performed using the IEFPCM[42−44] and SMD[45] models at the CASSCF level, which were denoted IEFPCM/CASSCF and SMD/CASSCF, respectively, to investigate the mechanism of excited-state proton transfer in solution. In the IEFPCM calculations, all of the hydrogen atoms have individual spheres and atomic radii from the UFF force field were scaled by 1.1. The self-consistent PCM (SC-PCM) calculations, which make the electrostatic potential generated by the excited-state density self-consistent with the solvent reaction field, were also performed for IEFPCM energies at the CASSCF level.[46,47] The SMD is a universal continuum solvation model to calculate the standard-state solvation free energy based on the bulk electrostatic

contribution arising from the SCRF treatment of the IEFPCM model and the contribution arising from short-range interactions between the solute and solvent molecules in the first solvation shell, which is called the cavity-dispersion-solvent-structure (CDS) term.[45] The CDS term, which is determined semiempirically, includes cavitation, dispersion, the partial covalent character of hydrogen bonding, and the deviation of the effective dielectric constant in the first solvation shell from its bulk value. Nonpolar heptane solvent was chosen for solution calculations to allow comparisons of the theoretical and experimental results.[20] The geometries of reactant, product, and TS were completely optimized in heptane.

The multidimensional surface of the excited-state PMF along the reaction coordinates in solution were calculated for the first time using the equilibrium solvation path (ESP) approximation[48] at the MRPT2//SMD/CASSCF(10,9)/6-31G(d,p) level. The minimum energy path (MEP) is the steepest descent path in isoinertial solute cooordinates on a PMF, which is given by

$$U(\mathbf{R}|T) = V(\mathbf{R}) + \Delta G_S^0(\mathbf{R}|T) \tag{1}$$

where $U(\mathbf{R}|T)$ is the solution-phase potential of mean force as a function of solute coordinate $\mathbf{R}$ and temperature T, and $V(\mathbf{R})$ and $\Delta G_S^0(\mathbf{R}|T)$ are the gas-phase potential energy and the standard-state free energy of solvation for solute, respectively, in the zero-order cannonical mean shape approximation.[48,49] The saddle point on this multidimensional solute surface of PMF will be called the conventional TS. The reaction coordinate parameter s is the signed distance from the TS along the MEP in isoinertial solute coordinates. The solution-phase standard-state free energy of solute is given by

$$G^0(\mathbf{R}_s|T) = U(\mathbf{R}_s|T) + G_{\mathrm{RVE}}(\mathbf{R}_s|T) \tag{2}$$

where $G_{\mathrm{RVE}}(\mathbf{R}_s|T)$ is the rovibrational internal free energy of solute species at position s on the reaction path ($s = -\infty$, $+\infty$, and 0 for reactant, product, and TS, respectively). In the ESP approximation, $G_{\mathrm{RVE}}(\mathbf{R}_s|T)$ is evaluated from the potential of mean force $U(\mathbf{R}_s|T)$.

The PMF curve $U(\mathbf{R}_s|T)$ along the reaction coordinate was calculated at the SMD/CASSCF level. Currently, the solvent effect is not implemented in MRPT2 calculations; therefore, the PMF curve $U(\mathbf{R}_s|T)$ in solution at the MRPT2 level was calculated by using gas phase MRPT2 energies for $V(\mathbf{R}_s)$ in eq 1 and solvation energies $\Delta G_S^0(\mathbf{R}_s|T)$ at the SMD/CASSCF level based on the interpolated VTST by mapping[32] (IVTST-M) algorithm. In this algorithm, 32 excited-state Hessian and 320 energy and gradient points along the MEP were used initially to construct the PMF and effective vibrationally adiabatic energy curves at the SMD/CASSCF level. This PMF curve in the excited state was corrected by 32 interpolated single point energies (ISPEs)[50] along the MEP at the MRPT2 level such that interpolation could generate the high-level PMF points that are required for rate constant calculations. These nonstationary Hessian and high-level energy points were chosen every 0.1 bohr between −2.0 and 1.2 bohr along the MEP at the SMD/CASSCF level. Therefore, the final excited-state PMF curves along the MEP in this study were obtained at the dual level, *i.e.*, the interpolated MRPT2//SMD/CASSCF-(10,9)/6-31G(d,p). The active spaces of all species along the reaction coordinate were consistently maintained with those of TS in the CASSCF and MRPT2 calculations.

The variational transition state is located at the position on the MEP where the standard-state generalized free energy of activation is a maximum. All vibrational energies are from solution-phase frequencies at the SMD/CASSCF level. The cannonical variational theory (CVT) rate constant is given by[48]

$$k^{\mathrm{CVT}} = \frac{k_B T}{hC^\circ} \exp[-\Delta G^{\mathrm{CVT},0}/RT] \tag{3}$$

where k_B is the Boltzmann constant; h is Planck's constant; C° is the concentration (1 molar) corresponding to the standard state; R is the gas constant; and $\Delta G^{\mathrm{CVT},0}$ is the standard state free energy of activation, which is a maximum along s of $\Delta G(\mathrm{GT}, s|T)$.

In order to consider tunneling, $k^{\mathrm{CVT}}(\mathrm{T})$ is multiplied by a transmission coefficient, κ^{SCT}.

$$k^{\mathrm{CVT/SCT}}(\mathrm{T}) = \kappa^{\mathrm{SCT}}(\mathrm{T}) k^{\mathrm{CVT}}(\mathrm{T}) \tag{4}$$

The transmission coefficient is defined as the ratio of the thermally averaged quantal transmission probability, $P(\mathrm{E})$, to the thermally averaged classical transmission probability for the effective vibrationally adiabatic potential of mean force along the reaction coordinate, U^a, which is equal to $U(\mathbf{R})$ plus the local solute zero-point energy (the vibrationally adiabatic potential of mean force will be called adiabatic energy with concision)

$$\kappa(T) = \frac{\int_0^\infty P(E) \exp(-E/k_B T) dE}{\int_{U^a[s_*^{\mathrm{CVT}}(T)]}^\infty \exp(-E/k_B T) dE} \tag{5}$$

This equation can be reduced to

$$\kappa(T) = \frac{1}{k_B T} e^{U^a[s_*^{\mathrm{CVT}}(T)]/k_B T} \int_0^\infty P(E) e^{-E/k_B T} dE \tag{6}$$

which can be written as

$$\kappa(T) = \frac{1}{k_B T} \kappa^{\mathrm{CVT/CAG}} \int_0^\infty [P(E) e^{U^{\mathrm{AG}}/k_B T}] e^{-E/k_B T} dE \tag{7}$$

where

$$\kappa^{\mathrm{CVT/CAG}} = e^{[U^a(s_*^{\mathrm{CVT}}) - U^{\mathrm{AG}}]/k_B T} \tag{8}$$

In eqs 7 and 8, $[P(E)e^{-E/k_B T}]e^{U^{\mathrm{AG}}/k_B T}$ is the thermally weighted quantal transmission probability scaled by $e^{U^{\mathrm{AG}}/k_B T}$, $U^a(s_*^{CVT})$ is the adiabatic energy barrier evaluated at the canonical variational transition state, and U^{AG} is defined as

$$U^{\mathrm{AG}} = \max_s U^a(s) \tag{9}$$

The centrifugal-dominant small-curvature semiclassical adiabatic ground state (CD-SCSAG) tunneling approximation[51−53] was used to calculate $P(\mathrm{E})$ for the process known as small-curvature tunneling (SCT). All rate calculations were carried out using the Gaussrate[54] program, which is an interface of the Gaussian[34] and Polyrate[55] dynamics programs. The $\Delta G_S^0(\mathbf{R}|T)$ solvation energies for 32 MRPT2 energy points were calculated by using the GESOL program.[56]

3. RESULTS AND DISCUSSION

3.1. Electronic Structures and Energetics of 7AI-CH_3OH and 7AI-C_2H_5OH Complexes. Structural parameters for the 7AI-C_2H_5OH complex optimized at the CASSCF(10,9)/6-31G(d,p) level in the gas phase are shown in Table 1 in

dx.doi.org/10.1021/ct3010694 | J. Chem. Theory Comput. 2013, 9, 3557−3566

Table 1. Bond Distances (Å) of Reactant and TS for the ESDPT of 7AI-CH_3OH and 7AI-C_2H_5OH Complexes in the Gas Phase at the CASSCF/6-31G(d,p) Level[a]

	CH_3OH		C_2H_5OH	
	reactant	TS	reactant	TS
$r(N_1-H_{10})$	0.998	1.288	0.998	1.292
$r(O_{16}-H_{10})$	2.147	1.187	2.147	1.184
$r(O_{16}-H_{17})$	0.951	1.035	0.951	1.029
$r(N_6-H_{17})$	2.112	1.557	2.117	1.578

[a]Numbering system of atoms is depicted in Scheme 1.

comparison with parameters of the 7AI-CH_3OH complex.[22] N−H and O−H bond distances in the reactant of the 7AI-CH_3OH and 7AI-C_2H_5OH complexes were almost identical. In the TS, the H_{10} atom moved more than the H_{17} atom, which resulted in a $C_2H_5OH_2^+$-like moiety. The ESDPT for 7AI-C_2H_5OH also occurred in a concerted but asynchronous process without an intermediate. Comparing the structural parameters for the TS of the 7AI-C_2H_5OH and 7AI-CH_3OH complexes,[22] the N_1-H_{10} and N_6-H_{17} distances of the 7AI-C_2H_5OH complex were longer, whereas the $O_{16}-H_{10}$ and $O_{16}-H_{17}$ distances were slightly shorter. These geometrical changes of the TS could be attributed to the higher basicity (gas-phase proton affinity) of ethanol as compared to methanol.[57]

Barrier heights ($\Delta V^{\ddagger}$) for the ESDPT of 7AI-CH_3OH and 7AI-C_2H_5OH complexes are listed in Table 2. Dynamic

Table 2. Barrier Heights (kcal/mol) for the ESDPT of 7AI-CH_3OH and 7AI-C_2H_5OH in the Gas Phase and in Heptane[a]

	CASSCF	MRPT2
	7AI-CH_3OH	
gas phase	17.1(13.7)	8.71(5.31)
IEFPCM	19.5(16.7)	12.0(9.12)
SC-PCM[b]	15.8(12.9)	8.23(5.40)
SMD[c]	13.4(10.6)	5.83(3.05)
SMD-G[d]	15.4(12.6)	7.87(5.09)
	7AI-C_2H_5OH	
gas phase	17.1(13.8)	8.79(5.43)
IEFPCM	22.7(19.9)	15.3(12.5)
SC-PCM[b]	15.7(12.9)	8.26(5.46)
SMD[c]	13.4(10.6)	5.93(3.19)
SMD-G[d]	15.6(12.8)	8.14(5.40)

[a]The numbers in parentheses include zero-point energies. Non-electrostatic terms were not included in the IEFPCM model. [b]The self-consistent PCM algorithm was used in the IEFPCM model. [c]SMD solvent model in G09. [d]SMD-G solvent model in GESOL with G03.

electron correlation decreased barrier heights significantly. The $\Delta V^{\ddagger}$ values of the ESDPT for 7AI-CH_3OH and 7AI-C_2H_5OH complexes were 5.31 and 5.43 kcal/mol, respectively, at the MRPT2 level including ZPEs in the gas phase. The ethanol complex has a slightly higher barrier in the gas phase than the methanol complex.

The excited state tautomerization for 7AI in bulk solvents[17,58−61] implies that solvent effects play a key role in proton transfer dynamics. The optimized structures of stationary points in heptane were confirmed by frequency calculations, as illustrated in Figure 1. Structural changes of the reactant and product in solution were nearly independent of the solvent model. The solvent effect increased the N−H

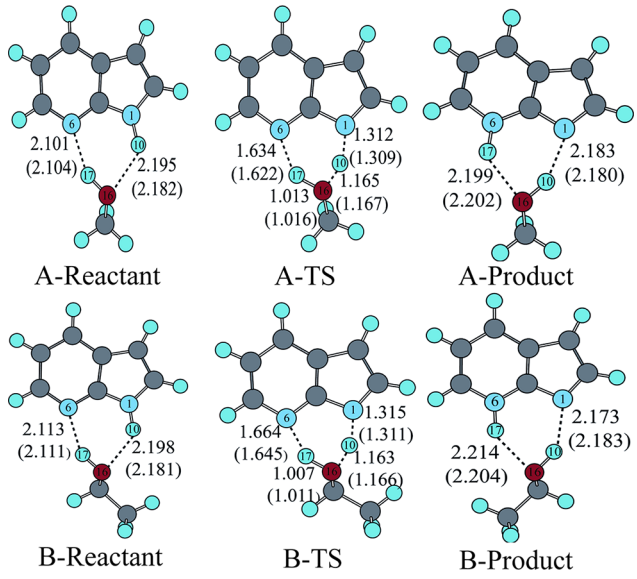

Figure 1. Reactant, product, and TS structures for the ESDPT of 7AI-CH_3OH and 7AI-C_2H_5OH optimized at the CASSCF(10,9)/6-31G(d,p) level with the SMD and IEFPCM (values in parentheses) models. A: 7AI-CH_3OH, B: 7AI-C_2H_5OH.

distances but decreased the O−H distances of the TS, compared with the corresponding distances in the gas phase, which results in more pronounced ion-pair character in the TS.

The barrier heights ($\Delta U^{\ddagger}$) for the ESDPT in heptane are also listed in Table 2. The $\Delta U^{\ddagger}$ values were highly dependent on the solvation model. When the IEFPCM was used, all $\Delta U^{\ddagger}$ values were larger than the corresponding gas phase values. These results are physically unreasonable because the solvent effect stabilizes the TS more than the reactant to reduce the barrier when the TS has a larger dipole moment than the reactant. Excited-state dipole moments in the gas phase and in solution are listed in Table S1. The dipole moments of the TS were larger than those of the reactants, and the differences were nearly the same irrespective of the solvent model, which should result in a similar solvent effect. The IEFPCM/CASSCF calculation in the G09 program[34] produced unreasonably positive solvation energy for hexane solvent, which is probably attributed to the fixed reaction field that is not self-consistently optimized (equilibrated) with the solute CASSCF wave functions.

The SC-PCM approach, which does an external iteration to calculate the solvent effect self-consistently with respect to the solute CASSCF density, addressed this problem; the IEFPCM $\Delta U^{\ddagger}$ values were reduced to become smaller than the gas phase values, as expected from the dipole moment changes between reactants and TS. The SC-PCM approach seems to be very important for excited-state calculations in solution with the IEFPCM model. Although the SC-PCM approach produced correct trends for the activation energies in solution, their $\Delta U^{\ddagger}$ values at the MRPT2 level were nearly the same as those in the gas phase. The ZPE-corrected activation energy at the MRPT2//SMD/CASSCF/6-31G(d,p) level was 3.1 kcal/mol for 7AI-CH_3OH, which is about 2 kcal/mol smaller than the gas phase value. This is consistent with experimental observations that the excited-state tautomerization of the 1:1 7AI:alcohol complex was only observed in solution and not in the gas phase.[9,11] However, although the SMD model predicted lower activation energies than SC-PCM, it had the same

dx.doi.org/10.1021/ct3010694 | J. Chem. Theory Comput. 2013, 9, 3557−3566

problem that produced positive solvation free energies; the reactant solvation energy was more positive than the TS, which resulted in the lower barrier. Because one of the main components of SMD solvent model is the bulk electrostatic contribution arising from the SCRF treatment of IEFPCM, it is not surprising that SMD and IEFPCM contain similar problems in G09. Although the IEFPCM and SMD methods have successfully been applied for the ground-state solvation energy and spectroscopic studies using TD-DFT, they have never been tested extensively with excited-state CASSCF calculations and should be used carefully. There is no such problem when we used the GESOL program[56] to calculate the SMD solvation free energies for reactant, TS, and 32 MRPT2 points on the reaction path. We denote these values as SMD-G in Table 2. The ZPE-corrected $\Delta U^{\ddagger}$ value at the SMD-G level was 5.09 at the MRPT2 level for 7AI-CH_3OH, which is only 0.22 smaller than the corresponding gas phase value. The solvent effect stabilized the TS more than the reactant because the TS has a greater dipole moment than the reactant, which reduced the activation energy of ESDPT to increase the rate even in a nonpolar solution. However, both SC-PCM and SMD-G models in this study seem to underestimate the solvation energy of excited-states with the CASSCF calculations; therefore, the activation energy was reduced very little.

Kwon et al.[20] found that the rate constants of 7AI-alcohol complexes were dependent on the acidity of the alcohol in heptane (see Supporting Information Table S2); thus, they proposed that the proton transfer of 7AI was triggered by initial transfer of a proton from the alcohol to the pyridine nitrogen of 7AI, forming a cationic 7AI intermediate species, and was completed by rapid proton transfer from the pyrrole nitrogen of the intermediate to the transient alkoxide. A rate dependence on acidity was also observed in the excited-state tautomerization of 7-hydroxyquinoline-alcohol complexes.[62] However, for both 7AI-CH_3OH and 7AI-C_2H_5OH complexes, we found that the proton transfer began with the H_{10} atom (pyrrole hydrogen), which traveled more than halfway along the reaction coordinate toward O_{16} in the TS, whereas the location of the H_{17} atom rarely changed, which indicates the opposite proton transfer pathway. In these opposing pathways, the ZPE-corrected activation energy of the 7AI-C_2H_5OH complex at the MRPT2 level with the SMD-G model was 0.31 kcal higher than the corresponding value of the 7AI-CH_3OH complex, which is consistent with the smaller rate constant for 7AI-C_2H_5OH than 7AI-CH_3OH.[20] These results indicate that in the TS, even without O−H bond dissociation, the higher the acidity of the alcohol, the lower the activation energy of proton transfer; therefore, the rate constant dependence on acidity should not be used as a criterion of the ESDPT mechanism in this case.

3.2. Potential Surfaces of Mean Force. The PMF surface in heptane along the MEP was calculated at the SMD/CASSCF(10,9)/6-31G(d,p) level followed by MRPT2 correction for dynamic electron correlation, which were depicted in Figure 2. The PMF curve near the top of the barrier decreased rapidly on the reactant-side and slowly on the product-side. No well for an intermediate appeared on the PMF curve. The conventional TS at the SMD/CASSCF level is represented as the maximum on the PMF curve along the MEP (a saddle point), where the mass-scaled reaction coordinate parameter s equals zero. The MRPT2 correction shifted this maximum toward the product-side at s = 0.29 bohr, to generate a new conventional TS at this point.

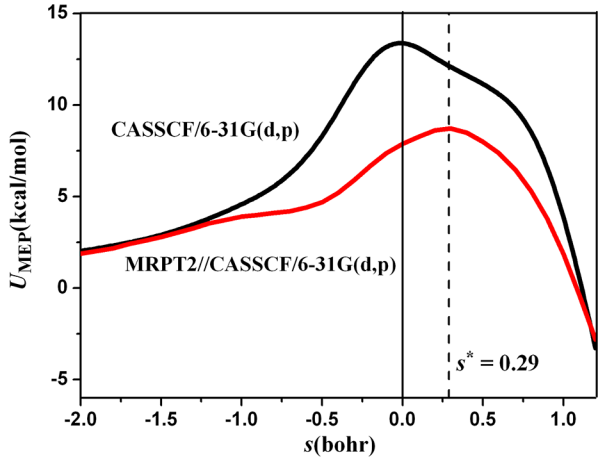

Figure 2. The PMF curves along the MEP of the 7AI-CH_3OH complex calculated at the SMD/CASSCF(10,9)/6-31G(d,p) and MRPT2//SMD-G/CASSCF(10,9)/6-31G(d,p) levels in heptane. The vertical solid and dashed lines represent saddle points (conventional TS) at the CASSCF (s = 0 bohr) and MRPT2 level (s = 0.29 bohr), respectively.

Dynamic electron correlation not only decreased the PMF barrier but also moved the saddle point obtained at the CASSCF level from its initial position (s = 0 bohr) toward the product region (s = 0.29 bohr). The O_{16}−H_{10} and N_6−H_{17} distances at s = 0.29 bohr were 0.121 Å and 0.050 Å shorter than those at s = 0 bohr, respectively. The H_{10} atom was shifted further toward the O_{16} atom compared with the H_{17} atom shifted toward the N_6 atom in the TS, which increases the asynchronicity of the ESDPT. The MRPT2 level PMF curve was smooth without any irregularity. The variational transition state theory can correctly take the new TS information (at s = 0.29 bohr) by the "variational" selection of TS and calculate the rate constant accordingly.

Changes in the N−H, O−H, and N−O bond distances along the reaction coordinate are shown in Figure 3. Relative bond distances for N_1−H_{10}, O_{16}−H_{17}, and N_1−O_{16} with respect to their equilibrium values in the reactant were obtained as well as the relative bond distances of O_{16}−H_{10} and N_6−H_{17} with

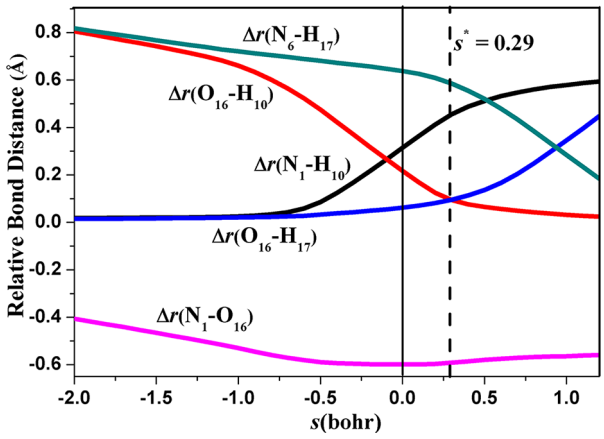

Figure 3. Selected relative bond distances along the reaction coordinate for the 7AI-CH_3OH complex calculated at the SMD/CASSCF(10,9)/6-31G(d,p) level in heptane. The vertical solid and dashed lines represent positions of the conventional TS at the CASSCF (s = 0 bohr) and MRPT2 level (s = 0.29 bohr), respectively.

dx.doi.org/10.1021/ct3010694 | J. Chem. Theory Comput. 2013, 9, 3557−3566

Table 3. Selected Bond Lengths in Å for the Reactant, Conventional TS, the Variational TS at 0 K in the S_1 State of 7AI-CH_3OH in Heptane with the SMD Model and the Relative PMF and Adiabatic Energies in kcal/mol

				VTS0[c]			
	R	TS[a] (0.0)[d]	TS[b] (0.29)[d]	$H_{10}H_{17}$ (0.31)[d]	$D_{10}H_{17}$ (0.31)[d]	$H_{10}D_{17}$ (0.31)[d]	$D_{10}D_{17}$ (0.41)[d]
N_1–H_{10}	0.998	1.312	1.450	1.457	1.457	1.457	1.448
O_{16}–H_{10}	2.195	1.165	1.044	1.041	1.041	1.041	1.048
O_{16}–H_{17}	0.951	1.013	1.046	1.041	1.041	1.041	1.044
N_6–H_{17}	2.101	1.634	1.584	1.593	1.593	1.593	1.583
ΔU^e	0.00	7.87	8.77	8.76	8.41	9.00	8.61
$\Delta(U^e$+ZPE)	0.00	5.09	6.73	6.74	6.64	7.71	7.57

[a]Conventional TS at the CASSCF level. [b]Conventional TS at the MRPT2 level. [c]Variational TS at 0 K. [d]Mass scaled reaction coordinates parameter s in bohr. [e]The PMF at the MRPT2 level.

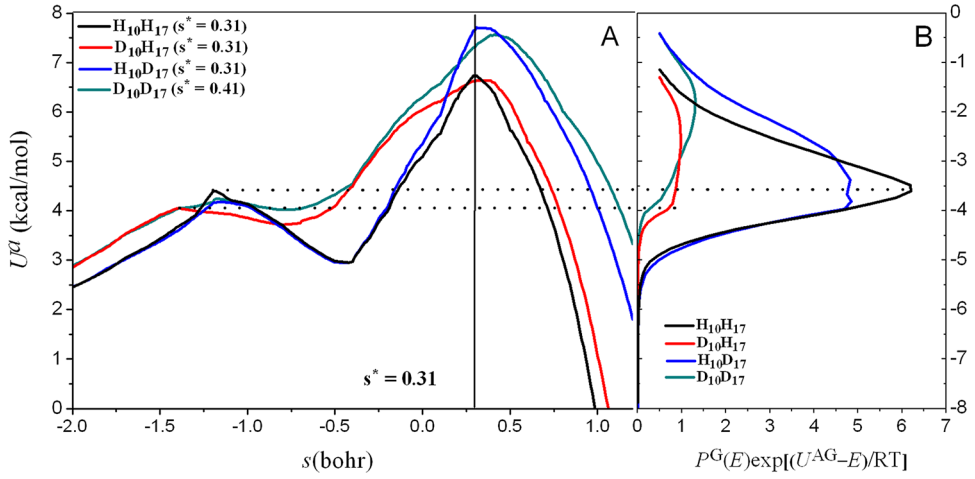

Figure 4. Adiabatic energy curves (A) along the MEP for isotopically substituted 7AI-CH_3OH complexes at the MRPT2 level in heptane and thermally weighted transmission probabilities (B) at 292 K scaled by $\exp(U^{AG}/RT)$ where U^{AG} is the adiabatic energy maximum. The vertical solid line represents the conventional TS at the MRPT2 level. The s* values in parentheses represent the positions of VTS0 on the MEP.

respect to their equilibrium product values. As ESDPT began from the reactant to product, the H_{10} atom moved rapidly to about $s = -0.8$ bohr from N_1 to O_{16}. The relative bond distance $\Delta r(N_1–H_{10})$ and $\Delta r(O_{16}–H_{10})$ values crossed near the conventional TS at about $s = -0.1$ bohr in the reactant region. Simultaneously, H_{17} moved very slowly from O_{16} to N_7, and the $\Delta r(O_{16}–H_{17})$ and $\Delta r(N_6–H_{17})$ values crossed at about $s = 0.95$ bohr in the product region. As a result, the transfer of H_{17} occurs mostly after the reaction has passed through the TS, which means that the two protons H_{10} and H_{17} are transferred highly asynchronously.

3.3. Adiabatic Energy Surfaces. The vibrational adiabatic energy is the sum of ZPEs and the PMF. The PMF decreases as the reaction goes from TS to either reactant or product. The ZPE change resulted from the frequency change of the vibrational modes, such as stretching and bending modes along the MEP. The decrease in the PMF and the increase in the ZPE are not necessarily in harmony. In particular, when the ZPE increases faster than the PMF decreases, the maximum in the adiabatic energy curve does not match the maximum of the PMF curve. The maximum of the adiabatic energy curve is the variational TS at 0 K, which is denoted as "VTS0" in this work. The structures, energies, and frequencies at the VTS0 are important for understanding the reaction dynamics, rate constants, and KIEs. The position of the VTS0 substantially depended on the isotopic substitution. In this study, the first hydrogen or deuterium represents H_{10} or D_{10}, respectively, and the second hydrogen or deuterium represents H_{17} or D_{17}, respectively, and the former and the later originated from solute and alcohol molecules, respectively.

Some structural parameters at the VTS0 and barriers for HH, DH, HD, and DD transfer are listed in Table 3 along with those of the saddle point ($s = 0$) at the CASSCF level. The VTS0 in the excited state did not occur near the CASSCF saddle points but near the MRPT2 points. The N_1–H_{10} and O_{16}–H_{17} distances of isotopomers at VTS0 were on average 0.14 and 0.03 Å longer, respectively, and the O_{16}–H_{10} and N_6–H_{17} distances were on average 0.12 and 0.04 Å shorter, respectively, than the corresponding values at the CASSCF saddle point. It is interesting to note that both O_{16}–H_{10} and O_{16}–H_{17} distances at the VTS0 were equal or less than 1.05 Å, which indicates that the $CH_3OH_2^+$ moiety is formed as part of the TS. These results strongly suggest that any study based only on the electronic structure calculation of stationary points even with dynamic electron correlation could not correctly model the ESDPT of 7AI-alcohol complexes in solution unless the PMF surfaces along the MEP are considered properly.

The adiabatic energies of the $H_{10}H_{17}$, $D_{10}H_{17}$, $H_{10}D_{17}$, and $D_{10}D_{17}$-substituted isotopomers at the MRPT2 level evaluated at $s = 0$ bohr (the saddle point of the CASSCF PMF surface) were 5.09, 6.04, 5.35, and 6.30 kcal/mol, respectively. The VTS0s for HH, DH, HD, and DD transfers appeared at s* = 0.31, 0.31, 0.31, and 0.41 bohr, respectively, with adiabatic energy barriers of 6.74, 6.64, 7.71, and 7.57 kcal/mol, respectively, at the MRPT2 level.

dx.doi.org/10.1021/ct3010694 | J. Chem. Theory Comput. 2013, 9, 3557–3566

Adiabatic energies along the excited-state MEP for isotopically substituted 7AI-CH_3OH complexes in heptane are shown in Figure 4A. Deuterium substitution for H_{10} (the pyrrole N−H) mostly widened the reactant-side of the barrier without increasing its height, whereas the substitution for H_{17} mostly widened the product-side of the barrier and increased the barrier height. These results mean that the isotopic substitution of alcohol raises the barrier height, whereas the substitution on solute widens the barrier. This phenomenon arises from ZPE changes along the asynchronous reaction coordinate that strongly depend on the position of isotope. The ZPE rapidly increases on the reactant-side, and a small hump appears on the product-side as depicted in Figure S1. It is also interesting that the shape of the hump in the relative ZPE curves depends on the position of isotope.

3.4. Rate Constants and Kinetic Isotope Effects. The rate constants including tunneling calculated by VTST/MT are listed in Table 4 for HH, DH, HD, and DD transfers. Quantum mechanical tunneling was expected to contribute significantly to the excited-state tautomerization of 7AI-CH_3OH complexes. The HH rate constants including tunneling $k^{CVT/SCT}$ were on the order of 10^7 s^{-1}, where tunneling gave a 6.3−44.6-fold increase in the rate constants. Kwon et al.[20] reported that k_{HH} and k_{DD} were 1.14×10^{10} s^{-1} and 7.81×10^8 s^{-1}, respectively. The rate constants obtained in this work were 100 times smaller than the experimental values due to the overestimated barrier height by about 3 kcal/mol. The calculated HH/DD KIE was 14.6 at 292 K, which is in excellent agreement with the experimental value (14.5).[20] The KIE was very sensitive to the TS properties and the shape of the adiabatic energy surfaces near the TS; therefore, the excellent agreement between experimental and theoretical KIEs strongly suggests that the PMF and adiabatic energy surfaces constructed in this study effectively represent the liquid phase ESDPT of 7AI. This study also suggests that the dynamics electron correlation by the MRPT2//CASSCF approach might not alter the reaction path significantly, although it changed the energy to shift the position of the TS along the reaction coordinate. The VTST/MT properly selected the "variational" TS and used the information of the PMF surfaces near the TS for the rate constants including tunneling; otherwise, no good agreement would be obtained.

Table 4. Rate Constants (s^{-1}) and Tunneling Coefficients for HH, DH, HD, and DD Transfers in the 7AI-CH_3OH Complex at 292 K in Heptane Using the SMD-G Model

	k^{CVT}	$k^{CVT/SCT}$	κ^{SCT}
$H_{10}H_{17}$	3.48×10^6	7.04×10^7	20.3
$D_{10}H_{17}$	3.62×10^6	1.79×10^7	4.94
$H_{10}D_{17}$	5.93×10^5	1.34×10^7	22.6
$D_{10}D_{17}$	7.23×10^5	4.80×10^6	6.64

For a concerted process, it is necessary but not sufficient to show that $k_{HD} = k_{DH}$ and that $k_{HD} = (k_{HH}\, k_{DD})^{1/2}$. The latter criterion is referred to as the "rule of the geometric mean (RGM)" originally stated by Bigeleisen.[63] The value of $k_{HD}^{CVT/SCT}$ (1.34×10^7 s^{-1}) at 292 K was smaller than $k_{DH}^{CVT/SCT}$ (1.79×10^7 s^{-1}) and was different from $(k_{HH}^{CVT/SCT}\, k_{DD}^{CVT/SCT})^{1/2}$ (5.81×10^7 s^{-1}), which indicates a breakdown of the RGM in the double proton transfer. Kwon et al.[20] also observed a breakdown of the RGM and suggested that the two protons move in succession. However, this breakdown can occur even in a concerted reaction when the two protons are transferred asynchronously.[64] The changes in bond distances and force constants at the TS for two protons in flight are very different in the asynchronous reaction, which results in the failure of the RGM. Thus, the breakdown of RGM cannot be used as evidence of a stepwise mechanism in this case.

The tunneling coefficients κ^{SCT} for $H_{10}H_{17}$, $D_{10}H_{17}$, $H_{10}D_{17}$, and $D_{10}D_{17}$ transfers were 20.3, 4.94, 22.6 and 6.64, respectively, at 292 K. It is very interesting that the tunneling coefficients of HD and DD transfers were slightly larger than those of HH and DH, respectively, which indicates that the isotopic substitution of solvent (hydroxyl proton) increases tunneling. Tunneling coefficients depended on the shape of the adiabatic energy surfaces along the MEP, which is shown in Figure 4A. The deuterium substitution of pyrrole N−H widened the reactant-side of the barrier without increasing its height, whereas the substitution of O−H widened the product-side of the adiabatic energy barrier and increased the barrier height to give more space for tunneling near the top of the barrier. The thermally weighted transmission probabilities (TPs) at 292 K are depicted in Figure 4B; tunneling coefficients depended on the area under the TP curves, which shows that tunneling is significant even at energies far below the adiabatic energy maximum. The area for DH was much smaller than for HH, which yielded smaller transmission coefficients for DH compared to HH due to the increased width of the adiabatic barrier upon deuterium substitution of the pyrrole N−H. However, the area for HD was slightly larger than HH, even though deuterium substitution of O−H also widened the product-side adiabatic barrier. The TP of HD near the barrier top was larger than that of HH due to the increased barrier height. The TP value of HH decreased very rapidly at $E \approx 4.4$ kcal/mol due to the small hump in the reactant-side of adiabatic energy curve at $s \approx -1.2$ bohr (Figure 4A) that greatly widened the energy barrier. Two TP curves for HH (black) and HD (blue) crossed at $E \approx 4.5$ kcal/mol, but the area of the HD curve was slightly larger than the area of the HH curve.

Figure 5 shows the pre- and post-tunneling configurations for the representative tunneling path (RTP)[65] at 292 K, which occurred between $s = -0.16$ and 0.68 bohr along the MEP, respectively. The RTP is where the TP is at a maximum. Between these two points, protons H_{10} and H_{17} moved 0.31 Å and 0.15 Å by tunneling from N_1 to O_{16} and from O_{16} to N_6, respectively. H_{10} traveled a longer distance by tunneling than

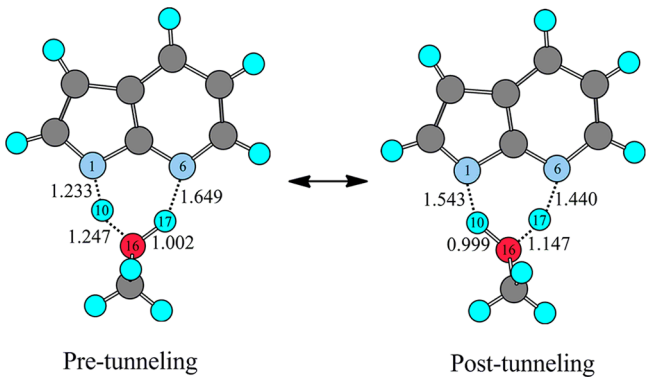

Figure 5. Pre- and post-tunneling configurations in the representative tunneling path at 292 K.

dx.doi.org/10.1021/ct3010694 | J. Chem. Theory Comput. 2013, 9, 3557−3566

H_{17}, which results in the stronger tunneling dependence of the isotopically substituted complex. Kwon et al.[20] found that the KIE decreased as the viscosity of the solvent increased and suggested that viscous solvent motion reduces tunneling because it diminishes the rate for reaching the pretunneling configuration of solute. Kwon et al.[20] also found from Arrhenius plots of k_{pt} that not only the rate constant k but also the KIE is independent of temperature within their experimental error and that the Arrhenius pre-exponential factor, $A(H)/A(D)$ was 37, which suggests that tunneling is very efficient for both isotopomers. When the tunneling contribution is large, the $A(H)/A(D)$ value is in general much less than unity. However, if tunneling becomes large enough to be equally effective for both H and D, then the ratio becomes much greater than unity. These types of temperature-independent Arrhenius plots have been reported for enzymatic proton transfers of lipoxygenase[66] and thermophilic alcohol dehydrogenase[7] and for solid-state porphyrins at low temperature.[67] Temperature-independent and large KIEs for enzymes have been explained with a model employing vibrationally enhanced proton tunneling[25] as originally suggested by Dogonadze et al.[25−27]

The calculated Arrhenius plots were linear as depicted in Figure S2, and the $A(HH)/A(DD)$ value was about 39, which was larger than unity, and in excellent agreement with the experimental value observed by Kwon et al.[20] However, we could not reproduce temperature independent Arrhenius plots of rate constants and KIE, although the $A(HH)/A(DD)$ and HH/DD KIE values were successfully predicted. The temperature independent KIEs have not been fully understood yet.[28−32] A gated motion[26] coupled to low-frequency modes along the reaction coordinate, which brings the donor and acceptor to the pretunneling configuration, was proposed to interpret temperature-independent KIEs. The enhancement of excited-state proton transfer rate in the 7AI complexes with water and methyl alcohols has been observed in the gas phase by the excitation of the gated motion.[10−12] The coupling of this gating motion with the hydrogenic motion is included in the multidimensional formalism of large curvature tunneling (LCT) approximation, which cannot be used for the interpolated PMF surfaces generated in this study. However, Pu et al.[31] reported that nearly temperature independent KIEs in condensed phase might originate from the variation of the TS position and the temperature dependent effective barrier for tunneling rather than the coupling of gating motion with tunneling. Glowacki et al.[28] proposed a two-state kinetic model for the temperature independent KIEs in enzyme, where the proton transfer occurs from two equilibrated conformers with different barriers.

We calculated a singly H-bonded complex in the excited-state as shown in Scheme 2, which has higher energy by 6.1 kcal/mol than the cyclic complex at the MRPT2 level. The initial excited-state conformer in heptane is mostly a cyclic complex, because it is the most stable structure in the ground-state. The conformational change from cyclic to noncyclic complex requires at least 6.1 kcal/mol of energy, which is smaller than the barrier of proton transfer. Although the barrier in this study is overestimated, it would be still possible that the conformational change might compete with the ESDPT. The conversion from the cyclic to noncyclic H-bonded complex requires the rotation of the methyl group, which would be independent of the isotopic substitution but highly dependent on the viscosity. Therefore, at high temperature the conformational change can

Scheme 2

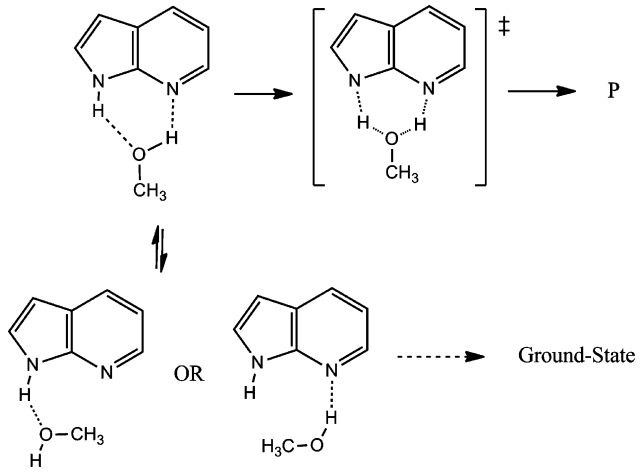

be faster due to lower viscosity, which may slow down the rate of the proton transfer. This competition becomes more significant for deuterium than hydrogen because the proton transfer rate is slowed down upon isotopic substitution, while the rate of conformational change remains the same. Further study would be necessary to fully understand the temperature independent rates and KIEs in the condensed phase and in enzyme.

4. CONCLUSIONS

We demonstrated that the excited state tautomerization of a 1:1 7AI-CH_3OH complex in nonpolar solution could be successfully investigated using variational transition state theory including multidimensional tunneling based on the quantum mechanically constructed surfaces of the potential of mean force (PMF). The PMF surfaces were generated at the MRPT2//SMD-G/CASSCF/6-31G(d,p) level using the IVTST-M algorithm with an interpolated single-point energy correction for dynamic electron correlation at 32 points along the reaction coordinate.

The IEFPCM model failed to reproduce the energetics of ESDPT in solution. The SC-PCM approach seems to be very important for solvent effects in the excited-state using the IEFPCM model. This study showed that any electronic structure calculation of stationary points in the excited-state even with dynamic electron correlation might not be able to correctly model the ESDPT of 7AI-alcohol complexes in solution without considering the PMF surfaces along the MEP.

The KIE values for the ESDPT of the 1:1 7AI-CH_3OH complex in heptane were in good agreement with the experimental results. The shape of the adiabatic energy surfaces in the excited-state strongly depended on the position of isotopes due to the asynchronicity of the reaction path, and the tunneling effect was essential for reproducing experimental KIEs. The isotopic substitution on alcohol slightly enhanced tunneling probability. This study revealed that the ESDPT in heptane occurs via a concerted but asynchronous mechanism.

The temperature independent Arrhenius behavior might be attributed to the conformational change from cyclic to noncyclic H-bonded complex, which depends on temperature, rather than the coupling of gated motion with tunneling, although further study would be necessary to fully understand.

dx.doi.org/10.1021/ct3010694 | J. Chem. Theory Comput. 2013, 9, 3557−3566

■ ASSOCIATED CONTENT

Supporting Information

Excited-state dipole moments in the gas phase and in solution are listed in Table S1. The acidity and basicity values for the alcohol and the alcohol-dependent ESDPT rate constants in heptane are listed in Table S2. Figure S1 shows the relative zero-point energies of isotopically substituted 7AI-CH_3OH complexes along the MEP in terms of the corresponding reactant values. Figure S2 shows the Arrhenius plots of HH and DD rate constants in heptane. This material is available free of charge via the Internet at http://pubs.acs.org.

■ AUTHOR INFORMATION

Corresponding Author

*E-mail: yhkim@khu.ac.kr.

Notes

The authors declare no competing financial interest.

■ ACKNOWLEDGMENTS

This work was supported by a grant from Kyung Hee University in 2012. We are pleased to acknowledge the support of the Center for Academic Computing at Kyung Hee University for computing resources.

■ REFERENCES

(1) Tuckerman, M. E.; Marx, D.; Parrinello, M. *Nature* **2002**, *417*, 925−929.
(2) Mohammed, O. F.; Pines, D.; Nibbering, E. T. J.; Pines, E. *Angew. Chem., Int. Ed.* **2007**, *46*, 1458−1461.
(3) Lill, M. A.; Helms, V. *Proc. Natl. Acad. Sci.* **2002**, *99*, 2778−2781.
(4) Mathias, G.; Marx, D. *Proc. Natl. Acad. Sci.* **2007**, *104*, 6980−6985.
(5) Faxen, K.; Gilderson, G.; Adelroth, P.; Brzezinski, P. *Nature* **2005**, *437*, 286−289.
(6) Lu, D.; Voth, G. A. *J. Am. Chem. Soc.* **1998**, *120*, 4006−4014.
(7) Kohen, A.; Cannio, R.; Bartolucci, S.; Klinman, J. P. *Nature* **1999**, *399*, 496−499.
(8) Hay, S.; Pudney, C. R.; McGrory, T. A.; Pang, J.; Sutcliffe, M. J.; Scrutton, N. S. *Angew. Chem., Int. Ed.* **2009**, *48*, 1452−1454.
(9) Sakota, K.; Komoto, Y.; Nakagaki, M.; Ishikawa, W.; Sekiya, H. *Chem. Phys. Lett.* **2007**, *435*, 1−4.
(10) Sakota, K.; Inoue, N.; Komoto, Y.; Sekiya, H. *J. Phys. Chem. A* **2007**, *111*, 4596−4603.
(11) Sakota, K.; Komure, N.; Ishikawa, W.; Sekiya, H. *J. Chem. Phys.* **2009**, *130*, 224307−7.
(12) Sakota, K.; Jouvet, C.; Dedonder, C.; Fujii, M.; Sekiya, H. *J. Phys. Chem. A* **2010**, *114*, 11161−11166.
(13) Koizumi, Y.; Jouvet, C.; Norihiro, T.; Ishiuchi, S. I.; Dedonder-Lardeux, C.; Fujii, M. *J. Chem. Phys.* **2008**, *129*, 104311−10.
(14) Pino, G. A.; Alata, I.; Dedonder, C.; Jouvet, C.; Sakota, K.; Sekiya, H. *Phys. Chem. Chem. Phys.* **2011**, *13*, 6325−6331.
(15) Yu, X.-f.; Yamazaki, S.; Taketsugu, T. *J. Phys. Chem. A* **2012**, *116*, 10566−10573.
(16) Daengngern, R.; Kungwan, N.; Wolschann, P.; Aquino, A. J. A.; Lischka, H.; Barbatti, M. *J. Phys. Chem. A* **2011**, *115*, 14129−14136.
(17) Moog, R. S.; Maroncelli, M. *J. Phys. Chem.* **1991**, *95*, 10359−10369.
(18) Mente, S.; Maroncelli, M. *J. Phys. Chem. A* **1998**, *102*, 3860−3876.
(19) Chou, P. T.; Yu, W. S.; Wei, C. Y.; Cheng, Y. M.; Yang, C. Y. *J. Am. Chem. Soc.* **2001**, *123*, 3599−3600.
(20) Kwon, O. H.; Lee, Y. S.; Park, H. J.; Kim, Y. H.; Jang, D. J. *Angew. Chem., Int. Ed.* **2004**, *43*, 5792−5796.
(21) Chen, Y.; Gai, F.; Petrich, J. W. *J. Am. Chem. Soc.* **1993**, *115*, 10158−10166.
(22) Fang, H.; Kim, Y. H. *J. Phys. Chem. A* **2011**, *115*, 13743−13752.
(23) Fang, H.; Kim, Y. H. *J. Phys. Chem. B* **2011**, *115*, 15048−15058.
(24) Kohen, A. *Prog. React. Kinet. Mech.* **2003**, *28*, 119−156.
(25) Dogonadze, R. R.; Kuznetsov, A. M.; Levich, V. G. *Electrochim. Acta* **1968**, *13*, 1025−1044.
(26) Kuznetsov, A. M.; Ulstrup, J. *Can. J. Chem.* **1999**, *77*, 1085−1096.
(27) Kornyshev, A. A.; Kuznetsov, A. M.; Stimming, U. *J. Chem. Phys.* **1997**, *106*, 9523−9528.
(28) Glowacki, D. R.; Harvey, J. N.; Mulholland, A. J. *Nat. Chem.* **2012**, *4*, 169−176.
(29) Hay, S.; Scrutton, N. S. *Nat. Chem.* **2012**, *4*, 161−168.
(30) Truhlar, D. G. *J. Phys. Org. Chem.* **2010**, *23*, 660−676.
(31) Pu, J.; Ma, S.; Gao, J.; Truhlar, D. G. *J. Phys. Chem. B* **2005**, *109*, 8551−8556.
(32) Pu, J.; Gao, J.; Truhlar, D. G. *Chem. Rev.* **2006**, *106*, 3140−3169.
(33) Corchado, J. C.; Coitiño, E. L.; Chuang, Y. Y.; Fast, P. L.; Truhlar, D. G. *J. Phys. Chem. A* **1998**, *102*, 2424−2438.
(34) Frisch, M. J.; Truck, G. W.; Schlegel, H. B.; Scuseria, G. E.; Robb, M. A.; Cheeseman, J. R.; Scalmani, G.; Barone, V.; Mennucci, B.; Petersson, G. A.; Nakatsuji, H.; Caricato, M.; Li, X.; Hratchian, H. P.; Izmaylov, A. F.; Bloino, J.; Zheng, G.; Sonnenberg, J. L.; Hada, M.; Ehara, M.; Toyota, K.; Fukuda, R.; Hasegawa, J.; Ishida, M.; Nakajima, T.; Honda, Y.; Kitao, O.; Nakai, H.; Vreven, T.; Montgomery, J. A., Jr.; Peralta, J. E.; Ogliaro, F.; Bearpark, M.; Heyd, J. J.; Brothers, E.; Kudin, K. N.; Staroverov, V. N.;Kobayashi, R.; Normand, J.; Raghavachari, K.; Rendell, A.; Burant, J. C.; Iyengar, S. S.; Tomasi, J.; Cossi, M.; Rega, N.; Millam, J. M.; Klene, M.; Knox, J. E.; Cross, J. B.; Bakken, V.; Adamo, C.; Jaramillo, J.; Gomperts, R.; Stratmann, R. E.; Yazyev, O.; Austin, A. J.; Cammi, R.; Pomelli, C.; Ochterski, J. W.; Martin, R. L.; Morokuma, K.; Zakrzewski, V. G.; Voth, G. A.; Salvador, P.; Dannenberg, J. J.; Dapprich, S.; Daniels, A. D.; Farkas, O.; Foresman, J. B.; Ortiz, J. V.; Cioslowski, J.; Fox, D. J. *Gaussian 09*; Gaussian, Inc.: Wallingford, CT, 2009.
(35) Nakano, H.; Nakayama, K.; Hirao, K.; Dupuis, M. *J. Chem. Phys.* **1997**, *106*, 4912−4917.
(36) Hirao, K. *Chem. Phys. Lett.* **1992**, *190*, 374−380.
(37) Hirao, K. *Chem. Phys. Lett.* **1992**, *196*, 397−403.
(38) Hirao, K. *Int. J. Quantum Chem.* **1992**, *S26*, 517−526.
(39) Hirao, K. *Chem. Phys. Lett.* **1993**, *201*, 59−66.
(40) Hashimoto, T.; Nakano, H.; Hirao, K. *J. Mol. Struct. (THEOCHEM)* **1998**, *451*, 25−33.
(41) Schmidt, M. W.; Baldridge, K. K.; Boatz, J. A.; Elbert, S. T.; Gordon, M. S.; Jensen, J. H.; Koseki, S.; Matsunaga, N.; Nguyen, K. A.; Su, S. J.; Windus, T. L.; Dupuis, M.; Montgomery, J. A. *J. Comput. Chem.* **1993**, *14*, 1347−1363.
(42) Cancès, E.; Mennucci, B.; Tomasi, J. *J. Chem. Phys.* **1997**, *107*, 3032−3041.
(43) Cossi, M.; Barone, V.; Mennucci, B.; Tomasi, J. *Chem. Phys. Lett.* **1998**, *286*, 253−260.
(44) Mennucci, B.; Tomasi, J. *J. Chem. Phys.* **1997**, *106*, 5151−5158.
(45) Marenich, A. V.; Cramer, C. J.; Truhlar, D. G. *J. Phys. Chem. B* **2009**, *113*, 6378−6396.
(46) Improta, R.; Barone, V.; Scalmani, G.; Frisch, M. J. *J. Chem. Phys.* **2006**, *125*, 054103−9.
(47) Improta, R.; Scalmani, G.; Frisch, M. J.; Barone, V. *J. Chem. Phys.* **2007**, *127*, 074504−9.
(48) Chuang, Y. Y.; Cramer, C. J.; Truhlar, D. G. *Int. J. Quantum Chem.* **1998**, *70*, 887−896.
(49) Cramer, C. J.; Truhlar, D. G. *Chem. Rev.* **1999**, *99*, 2161−2200.
(50) Chuang, Y. Y.; Corchado, J. C.; Truhlar, D. G. *J. Phys. Chem. A* **1999**, *103*, 1140−1149.
(51) Liu, Y. P.; Lynch, G. C.; Truong, T. N.; Lu, D. H.; Truhlar, D. G.; Garrett, B. C. *J. Am. Chem. Soc.* **1993**, *115*, 2408−2424.
(52) Skodje, R. T.; Truhlar, D. G.; Garrett, B. C. *J. Phys. Chem.* **1981**, *85*, 3019−3023.
(53) Lu, D. H.; Truong, T. N.; Melissas, V. S.; Lynch, G. C.; Liu, Y. P.; Garrett, B. C.; Steckler, R.; Isaacson, A. D.; Rai, S. N.; Hancock, G. C.; Lauderdale, J. G.; Joseph, T.; Truhlar, D. G. *Comput. Phys. Commun.* **1992**, *71*, 235−262.

(54) Zheng, J. J.; Zhang, S. X.; Corchado, J. C.; Chuang, Y. Y.; Coitino, E. L.; Ellingson, B. A.; Truhlar, D. G. *Gaussrate-version 2009-A*; University of Minnesota: Minneapolis, MN, 2009.
(55) Zheng, J. J.; Zhang, S. X.; Lynch, B. J.; Corchado, J. C.; Chuang, Y. Y.; Fast, P. L.; Hu, W. P.; Liu, Y. P.; Lynch, G. C.; Nguyen, K. A.; Jackels, C. F.; Fernandez Ramos, A.; Ellingson, B. A.; Melissas, V. S.; Villa, J.; Rossi, I.; Coitino, E. L.; Pu, J. Z.; Albu, T. V.; Steckler, R.; Garrett, B. C.; Isaacson, A. D.; Truhlar, D. G. *Polyrate-version 2010-A*; University of Minnesota: Minneapolis, MN, 2010.
(56) Marenich, A. V.; Hawkins, G. D.; Liotard, D. A.; Cramer, C. J.; Truhlar, D. G. *GESOL− version 2008*; University of Minnesota, Minneapolis, 2008.
(57) Hunter, E. P.; Lias, S. G. *J. Phys. Chem. Ref. Data* **1998**, *27* (3), 413−656.
(58) McMorrow, D.; Aartsma, T. *Chem. Phys. Lett.* **1986**, *125*, 581−585.
(59) Koijnenberg, J.; Huizer, A. H.; Varma, C. A. G. O. *J. Chem. Soc., Faraday Trans. II* **1988**, *84*, 1163−1175.
(60) Smirnov, A. V.; English, D. S.; Rich, R. L.; Lane, J.; Teyton, L.; Schwabacher, A. W.; Luo, S.; Thornburg, R. W.; Petrich, J. W. *J. Phys. Chem. B* **1997**, *101*, 2758−2769.
(61) Taylor, C. A.; El-Bayoumi, M. A.; Kasha, M. *Proc. Natl. Acad. Sci.* **1969**, *63*, 253−260.
(62) Kohtani, S.; Tagami, A.; Nakagaki, R. *Chem. Phys. Lett.* **2000**, *316*, 88−93.
(63) Bigeleisen, J. *J. Chem. Phys.* **1955**, *23*, 2264−2267.
(64) Nam, K.; Kim, Y. *J. Chem. Phys.* **2009**, *130*, 144310−10.
(65) Kim, Y.; Truhlar, D. G.; Kreevoy, M. M. *J. Am. Chem. Soc.* **1991**, *113*, 7837−7847.
(66) Jonsson, T.; Glickman, M. H.; Sun, S. J.; Klinman, J. P. *J. Am. Chem. Soc.* **1996**, *118*, 10319−10320.
(67) Braun, J.; Schwesinger, R.; Williams, P. G.; Morimoto, H.; Wemmer, D. E.; Limbach, H. H. *J. Am. Chem. Soc.* **1996**, *118*, 11101−11110.